RSC Sustainability

ROYAL SOCIETY OF CHEMISTRY

PAPER

View Article Online
View Journal | View Issue

Cite this: *RSC Sustainability*, 2025, **3**, 3554

Functionalized poly(aspartic acid) hydrogel particles as carriers for covalent enzyme immobilization†

Johanna Meyer, [a] Lars-Erik Meyer, [a] Hadir Borg, [b] Dirk Dorfs [b] and Selin Kara *[ac]

Enzyme immobilization has been extensively studied to access higher enzyme stability and recyclability, enable continuous operations, and thus increase overall productivity in lab- and technical-scale processes. Among different immobilization methods, covalent immobilization on polymer surfaces can be the key to improved mass transport, reduced enzyme leaching, and faster conversions. Poly(aspartic acid) (PASP) hydrogels provide modifiable surface areas and the possibility of functionalization for introducing different linkers for covalent enzyme immobilization. PASP is an anionic polypeptide that is a highly versatile, biocompatible, and biodegradable polymer, hence a sustainable compound for its integration in enzyme immobilization design. Within this article, we present functionalized PASP hydrogel particles with glycidol (carrier I), ethylenediamine (carrier II), and glutaraldehyde (carrier III), and their in-depth characterization. These novel hydrogel-based enzyme carriers were applied to immobilize *Candida antarctica* lipase B (*Ca*lB). Despite the relatively low immobilization yield, the immobilized *Ca*lB on carrier II demonstrated a notable increase in stability with a 2.6-fold prolongation of its half-life from 454 ± 116 h to 1181 ± 350 h at 30 °C compared to the free enzyme. The proof-of-concept reaction of immobilized *Ca*lB on carrier II for the kinetic resolution of (*R*,*S*)-1-phenylethanolacetate demonstrated the potential for performing more than eight cycles without any significant reduction in the product yield. This corresponds to an operational time of over 200 hours, demonstrating the possible applicability of these hydrogel-based novel enzyme carriers.

Received 15th April 2025
Accepted 14th June 2025

DOI: 10.1039/d5su00280j

rsc.li/rscsus

Sustainability spotlight

The present study, entitled "Functionalized poly(aspartic acid) hydrogel particles as carriers for covalent enzyme immobilization", addresses the development of poly(aspartic acid) (PASP) based enzyme immobilization hydrogels that are tailored *via* different functionalizations. PASP is an anionic polypeptide that is a highly versatile, biocompatible, and biodegradable polymer, hence a sustainable compound for its integration in enzyme immobilization design. Next to the straightforward preparation of these biocompatible and biodegradable hydrogels, the efficient use of the designed materials for their repeated use (up to 7 seven cycles were demonstrated) for enzymatic applications indicates the great potential of these tailored new materials. The work overall covers the UN sustainability goals of at least these two SDGs: SDG 9 – industry, innovation, and infrastructure; SDG 12 – responsible consumption and production.

Introduction

The majority of applied biocatalytic industrial procedures involve heterogeneous catalysts using immobilized enzymes. Advantages such as enhanced enzyme stability, improved handling, enabled continuous flow systems, and easier product separation can be considered. Different forms of enzyme immobilization were described in the literature, such as (i) encapsulation/entrapment of the biocatalyst into a matrix, (ii) crosslinking of the enzyme, and (iii) binding the enzyme to a (porous) support.[1] A wide range of different materials can be applied as enzyme carrier matrices, such as inorganic carriers (silica, silica gels, metal oxides, or porous glass),[2] organic natural carriers (chitin, chitosan, starch, alginate, collagen, cellulose, or agar–agar),[3,4] and organic synthetic carriers (polyacrylamide, polyurethane, polypropylene, polystyrene, silicones, ion-exchange resins, or epoxy resins).[5]

Hydrogels, hydrophilic three-dimensional crosslinked polymeric structures, are also commonly seen as carriers for enzymes.[6] These polymers can absorb a high amount of water,

[a]*Institute of Technical Chemistry, Leibniz University Hannover, Callinstraße 5, 30167 Hannover, Germany. E-mail: selin.kara@iftc.uni-hannover.de*

[b]*Institute of Physical Chemistry and Electrochemistry, Leibniz University Hannover, Callinstraße 5, 30167 Hannover, Germany*

[c]*Biocatalysis and Bioprocessing Group, Department of Biological and Chemical Engineering, Gustav Wieds Vej 10, 8000 Aarhus, Denmark*

† Electronic supplementary information (ESI) available. See DOI: https://doi.org/10.1039/d5su00280j

enlarging their volume and mass, while retaining their shape. Hydrogels could provide the enzyme with the required aqueous microenvironment for biocatalytic reactions in non-aqueous media. Natural polymers are often used as the basis for enzyme carrier matrices. The advantage of these materials is that they are inherently biocompatible, non-toxic, biodegradable, mechanically flexible, sustainable, and renewable. Alginate is commonly used due to its low cost, non-toxicity, biocompatibility, and gelation under mild conditions by adding divalent cations such as calcium ions.[7] In various studies, the entrapped enzymes showed increased stability against changes in pH and temperature, and storage under different conditions, compared to the corresponding free enzyme, and excellent recyclability.[8–10] To increase the stability and activity in various organic solvents, the alginate beads can be coated with another more hydrophobic polymer, such as chitosan.[11]

Besides the clear advantages of these natural polymer matrices, challenges still remain, such as structural inhomogeneity and a lack of gelation control, as well as pre-gelling and post-gelling limitations must be mentioned here as well. To overcome these drawbacks, semi-synthetic or fully synthetic polymers were introduced to this field, which offer better material stiffness. Materials such as polyvinyl alcohol (polyPVA)-based carriers provide enhanced stiffness and better interactions between enzymes or cells and the matrix compared to natural polymers. These carriers are chemically and mechanically stable, addressing the drawbacks of natural polymers.[12] In contrast, hydrophilic polymers such as poly(-hydroxyethylmethacrylate) (polyHEMA) exhibit poor mechanical stability, risk of enzyme leaching, and can swell in water. To control swelling and improve strength, they are often copolymerized with hydrophobic monomers such as methyl methacrylate (MMA).[13] To enhance immobilization matrices, additional monomers and crosslinkers can be incorporated. Surface immobilization using spacers can bypass mass transport limitations.[12–14] Ayhan *et al.* demonstrated that modified non-porous poly(ethyleneglycol)diacrylate (polyPEGDA) and HEMA beads with spacers retained significant enzyme activity, indicating efficient mass transfer relative to reaction rates.[15] New advancements include polymerized ionic liquids (pILs) and polyelectrolytes, some of which also function as hydrogels.

Grollmisch *et al*. encapsulated lipase B from *Candida antarctica* (*Ca*lB) within fully synthetic pILs consisting of 1-vinyl-3-methylimidazolium bromide (VEtImBr) and *N*,*N*′-methylenebisacrylamide (MBAA).[16] The kinetic resolution of *rac*-1-phenyl ethanol with vinyl acetate in nonpolar solvents was studied, achieving nearly full conversions, high catalytic activities, and recyclability for ten cycles.

In a previous study, we entrapped unspecific peroxygenase (UPO; E.C. 1.11.2.1) in 3D printable synthetic polyelectrolyte hydrogels, consisting of [2-(acryloyloxy)ethyl]trimethylammonium chloride (AETMA) and PEGDA.[17,18]

Enzyme immobilization in hydrogels can rely solely on encapsulation without the formation of covalent bonds; however, this approach carries a risk of enzyme leaching and mass transfer limitations. To reduce this risk, covalent bonds can be formed between the enzyme surface and the hydrogel matrix. This approach utilizes functional groups such as amino, aldehyde, carboxyl, and epoxy groups present in materials such as cellulose, agarose, and dextran.[19,20]

To our knowledge, only a few examples of covalent immobilization on synthetic hydrogels are known in the literature. Zwitterionic microscale hydrogel beads, consisting of poly(-carboxybetaine) were synthesized by Erfani *et al*.[21] The immobilization was carried out between the carboxylic acid groups of the microbeads and the lysine residues of the protease chymotrypsin. The observed immobilization yield was up to 72%, and the immobilized enzyme retained its original activity after 10 reaction cycles.

Poly(aspartic acid) (PASP) is another interesting polymeric material based on anionic polypeptides, characterized by its versatility, biocompatibility, biodegradability, and the possible origin from renewable resources.[22] These polymers were modified and functionalized *via* the amine-reactive precursor poly(-succinimide) (PSI), holding great potential for designing and developing novel biomaterials.[23–28] Krisch *et al.* reported silica gel/alginate/PASP composite beads, absorbing *Ca*lB on functionalized silica gel particles, followed by an additional entrapment in the interpenetrating network of thiolated PASP and zinc ion crosslinked alginate.[3]

In the research field of covalent enzyme immobilization, functionalization or surface modification is often studied with chitosan, other natural polymers, or even porous glass. We have adapted these immobilization strategies to our synthetic PASP hydrogels to achieve the best of both worlds: on the one hand, sustainable polymers, mostly derived from natural origin, and on the other hand, a high degree of polymerization controllability and batch reproducibility, due to their synthetic origin. Here, another positive aspect is the precise activation of the matrix by functionalizing the polymeric surface.

Materials and methods

Materials

L-Aspartic acid (Sigma-Aldrich; ≥98%), mesitylene (Sigma-Aldrich; 98%), sulfolane (Sigma-Aldrich; for synthesis), phosphoric acid (ACS reagent; ≥85 wt% in water), *N*,*N*′-dimethylformamide (DMF; VWR Chemicals; peptide synthesis), dimethylsulfoxide (DMSO; Supelco; EMSURE®, ACS, for synthesis), methanol (Sigma-Aldrich; for synthesis), ethylenediamine (Sigma-Aldrich; for synthesis), dibutylamine (Sigma-Aldrich; ≥99.5%); imidazole (Merck, buffer substance), sodium hydroxide (NaOH; Carl Roth; ≥99%), sodium borohydride (Thermo Scientific; 99.0%), glycidol (Sigma-Aldrich; 96%), sodium periodate (Sigma-Aldrich; ≥99.8%), sodium hydrogen carbonate (Carl Roth; ≥99.5%), glutardialdehyde (Sigma-Aldrich; 50% solution in water; for synthesis), Triton X-100 (Sigma-Aldrich; for molecular biology), trisodium phosphate (Sigma-Aldrich; buffer substance), 1-ethyl-3-(3-dimethylaminopropyl)carbodiimide hydrochloride (EDC; TCI; >98%), *N*-hydroxysuccinimide (NHS, TCI, >98%), 4-nitrophenylacetate (Sigma-Aldrich; esterase substrate), 4-nitrophenol (Sigma-Aldrich; ReagentPlus®, ≥99.0%), potassium hydrogenphosphate (Sigma-Aldrich; buffer substance), potassium

dihydrogenphosphate (Sigma-Aldrich; buffer substance), (*R*)-1-phenylethanolacetate (Sigma-Aldrich; ReagentPlus®, ≥99.0%), (*S*)-1-phenylethanolacetate (Sigma-Aldrich; ReagentPlus®, ≥99.0%), (*R*)-1-phenylethanol (Sigma-Aldrich; ReagentPlus®, ≥99.0%) and (*S*)-1-phenylethanolacetate (Sigma-Aldrich; ReagentPlus®, ≥99.0%) were used as received. Recombinant *Ca*lB (PDB code 1TCA, EC 3.1.1.3 triacylglycerol lipase) from c-LEcta GmbH was used as a biocatalyst throughout this study.

Synthetic procedures of the immobilization matrix

Synthesis of polysuccinimide (PSI, 2). The precursor polymer of poly(aspartic acid) (PASP) was synthesized by thermal polycondensation according to previously reported procedures (Scheme 1).[26,29,30] In short, aspartic acid was suspended in a mixture of mesitylene and sulfolane (7/3 weight ratio) at 160 °C with 85% H_3PO_4 as a catalyst (with a molar ratio of 16% H_3PO_4 to aspartic acid). After 7 h, the resulting polymer was filtered off from the reaction mixture, dissolved in DMF, and the remaining aspartic acid was filtered off. For precipitation, an excess of ultrapure water was added, and the obtained crude product was washed with ultrapure water and MeOH until the permeate yielded pH 6. The crude precipitate was dissolved in DMF, filtered, recrystallized under reduced pressure using a rotary evaporator, and dried at 80 °C (yield 83%).

The chemical structure was confirmed by ^{1}H NMR (400 MHz, DMSO-d_6, ppm; $\delta = 2.71$ (s, 1H, CH_2); 3.21 (s, 1H, CH_2); 5.27 (s, 1H, CH)), ^{13}C NMR (400 MHz, DMSO-d_6, ppm; $\delta = 32.7$ (s, CH_2); 47.4 (t, CH); 172.3 (q, CO); 173.5 (q, CO)), IR (cm^{-1}; $\tilde{\nu} = 1385$ (ν, C–H); 1655 (ν, C=O); 1705 (ν, C=O); 2945 (ν, C–H)) and Raman (cm^{-1}; $\lambda = 785$ nm; $\tilde{\nu} = 640$ (δ, C–H); 700 (δ, C–H); 775 (δ, C–C); 875 (δ, C–O); 1400 (ν, CO–N); 1800 (ν, C=O)). The average molecular weight of the PSI was determined by HPLC size-exclusion chromatography (SEC) with a PSS SDV precolumn (50 mm length; 8.0 mm diameter; 5 μm particle size) and two PSS SDV columns connected in a row (300 mm length; 8 mm diameter; 5 μm particle size; average molecular weight ranges from 0.1–60 kDa (column I) and 0.5–700 kDa (column II) with THF as an eluent. The average molecular weight of PASP was calculated to be $M_W = 68.8$ kDa with a polydispersity index (PDI) of 1.71.

Synthesis of poly(aspartic acid) hydrogels (PASP, 4). The hydrogels synthesis was adapted from Szilágyi *et al.* (Scheme 2).[30] PSI **2** (150 μmol) and ethylenediamine (EDA; 25 μmol) were dissolved in DMSO (100 μL). Crosslinking was initiated by adding dibutylamine (DBA; 60 μmol), followed by mixing and filling into molds and then resting at room temperature overnight. Afterward, the obtained PSI hydrogels **3** were hydrolyzed to PASP hydrogels **4** in a mildly alkaline solution (imidazole buffer; 250 mM; pH = 8) for three days while substituting the buffer every 24 h. The PASP hydrogel particles **4** were washed in ultrapure water and lyophilized. The particles were ground again in a mortar to yield an even higher surface area and tinier hydrogel particles.

The chemical structure was confirmed by IR (cm^{-1}; $\tilde{\nu} = 1387$ (ν, C–H); 1519 (ν, C=O); 1587 (δ, N–H); 1641 (ν, C=O); 2937 (ν, C–H); 3066 (ν, COO–H); 3265 (ν, N–H)) and Raman (cm^{-1}; $\lambda = 785$ nm; $\tilde{\nu} = 640$ (δ, C–H); 700 (δ, C–H); 775 (δ, C–C); 1400 (ν, CO–N); 1800 (ν, C=O)).

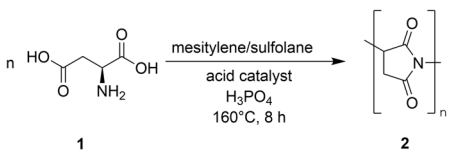

1 2

Scheme 1 Thermal polycondensation of aspartic acid **1** to polysuccinimide (PSI) **2**.

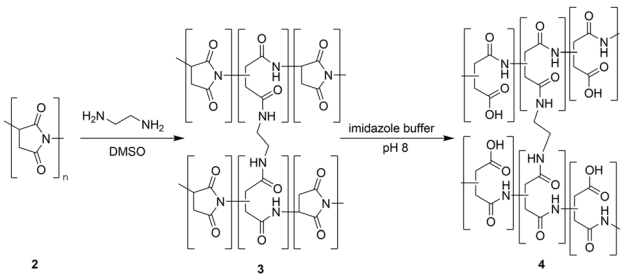

2 3 4

Scheme 2 The polysuccinimide (PSI) **2** was crosslinked with ethylenediamine to a polysuccinimide gel **3**, followed by alkaline hydrolysis to the poly(aspartic acid) (PASP) hydrogel **4**.

Functionalization of the PASP carrier I (EDC/NHS activated)

The PASP-hydrogel particles **4** were activated with 1-ethyl-3-(3-dimethylaminopropyl)carbodiimide hydrochloride/*N*-hydroxysuccinimide (EDC·HCl/NHS). The methodology was adapted from already reported procedures on the water-based functionalization of gelatine (Scheme 3).[31] In short, 5 mL of an aqueous EDC·HCl/NHS mixture (1 : 2 mol L^{-1}) and 0.1 g dry PASP hydrogel particles **4** were stirred at room temperature for 16 h to yield EDC/NHS activated PASP hydrogel particles **5**. Afterwards, **5** was filtered off and washed with ultrapure water. The wet hydrogel (PASP-EDC/NHS) **5** was directly used for further activation reactions for carrier II or immediately used to immobilize *Ca*lB as carrier I.

The chemical structure was confirmed by IR (cm^{-1}; $\tilde{\nu} = 1379$ (ν, C–H); 1510 (ν, C=O); 1639 (ν, C=O); 1718 (ν, C=O); 2937 (ν, C–H); 3066 (ν, COO–H); 3294 (ν, N–H)) and Raman (cm^{-1}; $\lambda = 785$ nm; $\tilde{\nu} = 640$ (δ, C–H); 725 (δ, C–H); 775 (δ, C–C); 1200–1400 (ν, C=O and CO–N); 1450 (ν, CO–N); 1800 (ν, C=O)).

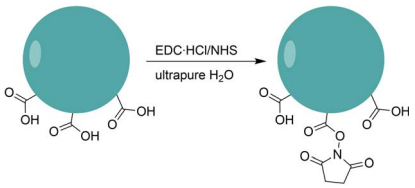

4 5

Scheme 3 1-Ethyl-3-(3-dimethylaminopropyl)carbodiimide hydrochloride (EDC·HCl) and *N*-hydroxysuccinimide (NHS) activation of PASP-hydrogels **4** to the NHS-ester activated PASP **5**.

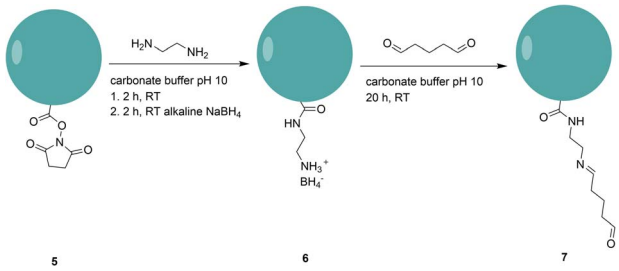

Scheme 4 The NHS-ester activated PASP **5** was functionalized first with ethylenediamine to PASP-EDA **6**, and further functionalized with glutaraldehyde to PASP-EDA-GLU **7**.

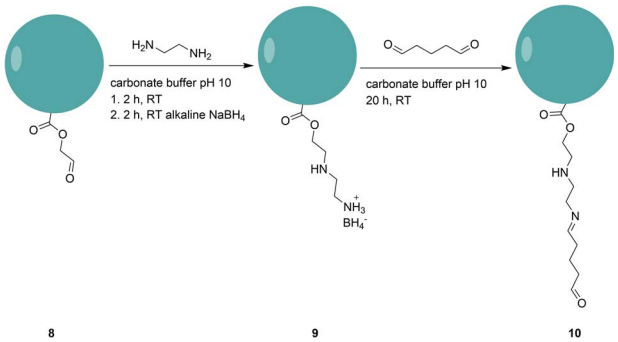

Scheme 6 The further functionalization of the glycidol activated PASP-GLY **8** with ethylenediamine to PASP-GLY-EDA **9** and with glutaraldehyde to PASP-GLY-EDA-GLU **10**.

Functionalization of the PASP carrier II (PASP-EDA-GLU)

The following procedure was adapted from a chitosan immobilization technique reported by Bonazza *et al.* (Scheme 4).[32] The NHS-ester activated PASP particles **5** (0.1 g) were suspended in a carbonate buffer (pH 10; 100 mM; 3.8 mL) with EDA (0.8 mmol) and stirred for 2 h at room temperature. The obtained gel particles were subsequently reduced for 2 h at room temperature with alkaline $NaBH_4$ (2.1 mL; 1.7 M NaOH; 5.55 M $NaBH_4$). After the filtration and washing of the hydrogel particles with ultrapure water, carbonate buffer (pH 10; 100 mM; 2.9 mL) and glutaraldehyde (150 μL; 50 wt%) were added. The suspension was stirred moderately for 20 h. The yielded particles (PASP-GLY-EDA-GLU) **7** were filtered, washed with ultrapure water, and immediately used to immobilize *Ca*lB.

The chemical structure of **6** was confirmed by IR (cm^{-1}; $\tilde{\nu}$ = 1037 (ν, C–C); 1101 (ν, C–N); 1384 (ν, C–H); 1521 (ν, C═O); 1595 (ν, C═O); 1643 (ν, C═O); 2864 (ν, C–H); 2924 (ν, COO–H); 3072 (ν, N–H); 3277 (ν, N–H)). The chemical structure of **7** was confirmed by IR (cm^{-1}; $\tilde{\nu}$ = 1375 (ν, C–H); 1517 (ν, C═O); 1637 (ν, C═O); 1705 (ν, C═O); 2943 (ν, C–H); 3061 (ν, COO–H); 3298 (ν, N–H)).

Functionalization of the PASP carrier III (PASP-GLY-EDA-GLU)

Glycidol-functionalization of the PASP hydrogel particles (PASP-GLY). The PASP hydrogel particles **4** were activated with glycidol. The methodology was adapted from procedures already reported on the activation of chitosan (Scheme 5).[32–34] In short, the PASP hydrogel particles **4** (0.4 g) were suspended in ultrapure water (6.3 mL) and alkaline $NaBH_4$ solution (2.1 mL; 1.7 M NaOH; 5.55 M $NaBH_4$). The pH of the suspension was adjusted between 13–14 and placed in an ice bath with constant stirring. Afterwards, glycidol (2 mL; 30.21 mmol) was added dropwise to the reaction mixture. The suspension was stirred for 18 h at 25 °C. The solid was filtered off, washed with ultrapure water, and stirred for 2 h in a sodium periodate solution (0.1 M; 10 mL) at 25 °C. The PASP-GLY hydrogel particles **8** were filtered off and washed with ultrapure water.

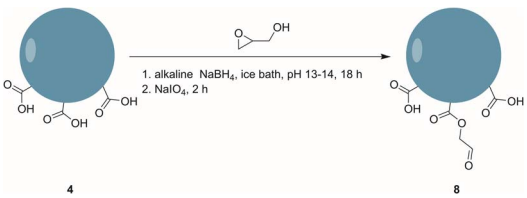

Scheme 5 The PASP hydrogel particles **4** were functionalized with glycidol to PASP-GLY **8**.

The chemical structure was confirmed by IR (cm^{-1}; $\tilde{\nu}$ = 1388 (ν, C–H); 1521 (ν, C═O); 1579 (δ, N–H); 1636 (ν, C═O); 2941 (ν, C–H); 3074 (ν, COO–H); 3271 (ν, N–H)) and Raman (cm^{-1}; λ = 785 nm; λ = 785 nm; $\tilde{\nu}$ = 900 (ν, C–C); 1000 (δ, C–H); 1200–1450 (ν, C═O and CO–N); 1675 (ν, C═O)).

EDA and glutardialdehyde-functionalization of the PASP-GLY hydrogel particles (PASP-GLY-EDA-GLU). The PASP-GLY particles **8** were functionalized with EDA and glutaraldehyde according to the procedure used for carrier II (PASP-EDA-GLU), yielding carrier III, which was immediately used for the immobilization of *Ca*lB (Scheme 6).

To confirm the structure of the borohydride adduct **9**, non-crosslinked PASP was functionalized according to the procedure described above and measured by ^{1}H NMR (400 MHz, D_2O, ppm; δ = −0.10 (q/sep, 4H, BH_4^-); 2.02 (ds, CH_2); 2.64 (s, CH_2); 2.77 (s, CH_2); 3.06 (s, CH_2); 3.24 (s, CH_2N); 3.59 (s, OCH_2); 4.24 (s, CH); 4.48 (s, CH)) and ^{13}C NMR (400 MHz, D_2O, ppm; δ = 44.06 (s, CH_2); 45.44 (s, CH_2); 46.31 (s, CH_2); 47.31 (s, CH_2); 49.93 s, CH_2); 55.40 (s, OCH_2); 58.35 (t, CH); 171.37 (t, CON); 174.91 (q, COO); 178.61 (q, CON); 184.39 (q; COO)). Additionally, the structure of **9** was confirmed by IR (cm^{-1}; $\tilde{\nu}$ = 1037 (ν, C–C); 1101 (ν, C–N); 1384 (ν, C–H); 1521 (ν, C═O); 1595 (ν, C═O); 1643 (ν, C═O); 2864 (ν, C–H); 2924 (ν, COO–H); 3072 (ν, N–H); 3277 (ν, N–H)). The chemical structure of PASP-GLY-EDA-GLU **10** was confirmed by IR (cm^{-1}; $\tilde{\nu}$ = 1386 (ν, C–H); 1519 (ν, C═O); 1581 (ν, C═O); 1637 (ν, C═O); 2939 (ν, C–H); 3078 (ν, COO–H); 3275 (ν, N–H)).

Characterization of the hydrogel support

The NMR spectra were recorded on a Bruker ULTRASHIELD 400 MHz. DMSO-d_6 was calibrated to 2.49 (^{1}H) and 39.50 (^{13}C), and D_2O was calibrated to 4.80 (^{1}H). Fourier transform infrared spectroscopy (FTIR) spectra were recorded on a Specac Single reflection diamond ATR-Quest. Raman spectra of the samples were recorded on a Cora 5001 (Anton Paar GmbH, Scharnhausen, Germany).

Scanning electron microscopy (SEM). SEM was used to analyze the surface morphology of the hydrogel particles, which were dried for 48 h at 70 °C. Before imaging the samples with the SEM (S3400N, Hitachi, Japan), they were sputter-coated with Au/Pd for 45 s (SC7620 Sputter Coater). The images were taken with an acceleration voltage of 20 kV and a working distance of 10 mm using the ImageJ software (National Institutes of Health, Bethesda, MD, USA).

Determination of the swelling degree ($q_{m,\infty}$). The equilibrium swelling degrees of the hydrogel particles were determined by placing the particles in sodium phosphate buffer or ultrapure water for 24 h under mild shaking. After centrifuging and removing the excess solvent, the hydrogel particles were weighed. The swelling degree ($q_{m,\infty}$) of the hydrogels was calculated according to the following equation (eqn (1)),

$$q_{m,\infty} = \frac{W_\infty}{W_0} - 1 \quad (1)$$

where W_0 is the initial weight and W_∞ is the hydrogel weight after 24 h of equilibrium swelling.

X-ray photoelectron spectroscopy (XPS). A PHI VersaProbe III with a monochromated Al anode (photon energy: 1486.6 eV) operating at 25.2 W X-ray source power was used for XPS measurement. A pass energy of 224 eV was used for survey spectra measurements, while for high resolution 69 eV pass energy was used. The X-ray beam diameter was 100 μm. The samples were immobilized on double-sided tape on a 25 mm XPS sample holder. All samples were freeze-dried using a Christ Alpha 2–4 LSC plus freeze dryer prior to XPS measurements. Data analysis was performed using MultiPak version 9.8.0.19. All spectra were charge corrected using the C1s signal for adventitious carbon at 284.8 eV.

Immobilization of the lipase B from *Candida antarctica* (*Ca*lB) on the three different carriers and characterization of the immobilized enzymes

Photometric assay determining the enzyme activity. Photometric measurements were carried out with a Cary 60 UV-Vis spectrophotometer from Agilent (Santa Clara, United States) in 1 cm polystyrene cuvettes. All data are reported as mean ± standard deviation of triplicate measurements.

Volumetric enzyme activity assay of *Ca*lB. The activity of *Ca*lB was determined *via* the absorption at 400 nm from the hydrolysis of *p*-nitrophenyl acetate with the spectrophotometric quantification of *p*-nitrophenylate released over 60 s at 30 °C (Scheme 7).

The assay solution contained sodium phosphate buffer (890 μL; 100 mM; pH 7.5), *p*-nitrophenyl acetate (10 μL; 10 mM; in DMSO), and the enzyme dilution (100 μL). For the immobilized enzyme, the enzyme dilution consisted of 40 mg of the carrier in 1 mL sodium phosphate buffer. One unit (U) of enzyme activity is defined as the amount of enzyme releasing 1 μmol of 4-nitrophenolate per minute under standard assay conditions (eqn (2)):

$$\text{Activity}_{\text{vol.}}\left(\text{U mL}^{-1}\right) = \frac{\Delta\text{Abs}_{400\text{ nm}} \times \text{DF} \times V}{\varepsilon_{400\text{ nm}} \times v \times d} \quad (2)$$

$\Delta\text{Abs}_{400\text{ nm}}$ is defined as the measured absorbance at 400 nm over time, DF is the dilution factor, d is the cuvette thickness, V is the sample volume, v is the enzyme volume in the cuvette and $\varepsilon_{400\text{ nm}}$ is the molar extinction coefficient ($\varepsilon_{400\text{ nm}} = 13.27 \pm 1.30$ L × mmol^{-1} × cm^{-1} [*p*-nitrophenol acetate]). The activity of the immobilized enzyme was calculated with the following equation (eqn (3)):

$$\text{Activity}_{\text{immob.}}\left(\text{U g}_{\text{carrier}}{}^{-1}\right) = \frac{\Delta\text{Abs}_{400\text{ nm}} \times \text{DF} \times V}{\varepsilon_{400\text{ nm}} \times m_{\text{carrier}} \times d} \quad (3)$$

All measurements were performed with a reference cell containing the same solution without enzyme.

Immobilization of *Ca*lB. The enzyme immobilization was carried out under moderate rotation (10 rpm) at room temperature for 20 h in a carbonate buffer (100 mM, pH 10, 3.85 mL) containing 0.15% (v/v) Triton X-100 with 0.1 g of the PASP carriers (dried weight). The use of Triton X-100 permitted the enzyme's active center to be orientated towards the activated polymer particles. To this mixture, 172 μL (200 U) of the cell free extract (CFE) of *Ca*lB was added. The loaded material was filtered off and washed three times with sodium phosphate buffer (100 mM, pH 7.5, 4 mL). The chemical structure of carrier III with the immobilized enzyme was confirmed by IR (cm^{-1}; $\tilde{\nu}$ = 860 (δ, C–H); 943 (ν, C–C); 1072 (ν, C–O); 1157 (ν, C–N); 1388 (ν, C–H); 1517 (ν, C=O); 1591 (δ, N–H); 1649 (ν, C=O); 2931 (ν, C–H); 3068 (ν, COO–H); 3238 (ν, N–H)).

Assessment of the enzyme immobilization by enzyme leaching experiments. The leaching test was carried out with 100 mg of the loaded material and washed in sodium phosphate buffer (100 mM, pH 7.5, 4 mL) for 60 min in a rotator at 10 rpm. The enzyme activity of the supernatant (first residual solution after enzyme immobilization) and the washing solutions were analyzed *via* the enzyme-specific activity assay. The procedure was repeated until no enzyme activity could be detected. To ensure the absence of further enzyme leaching, the loaded material was washed again for 24 h while rotating at 10 rpm and then the enzyme activity was measured. The protein content in the filtrate was determined according to the Bradford method, using bovine serum albumin (BSA) as a standard.[35] Sodium dodecyl sulphate–polyacrylamide gel electrophoresis (SDS PAGE) was run to confirm the previous results of the activity assay.

Furthermore, the protein loading and the immobilization yield could be calculated using the following equations (eqn (4) and (5)):

$$\text{Protein loading}\ \left(\text{mg}_{\text{immo.}}\ \text{g}_{\text{carrier}}{}^{-1}\right) = \frac{m_{\text{offered}} - m_{\text{supernatant+wash}}}{m_{\text{carrier}}} \quad (4)$$

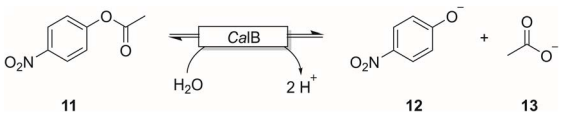

Scheme 7 Enzymatic hydrolysis reaction of *p*-nitrophenyl acetate (**11**) catalyzed by the enzyme *Ca*lB to *p*-nitrophenylate (**12**) and acetate (**13**).

$$\text{Immobilization yield (\%)} = \frac{m_{\text{offered}}(\text{mg}) - m_{\text{supernatant+wash}}(\text{mg})}{m_{\text{offered}}(\text{mg})} \times 100 \quad (5)$$

where m_{offered} is defined as the mass of the enzyme offered to the carrier for immobilization, and $m_{\text{supernatant+wash}}$ is defined as the mass of the enzyme in the supernatant and the wash fractions after the immobilization. By correlating the volumetric activity and the protein loading, the mass-specific activity (eqn (6)) and the activity yield (eqn (7)) can be calculated:

$$\text{Activity}_{\text{spec.}}\left(\text{U mg}_{\text{immo. enzyme}}{}^{-1}\right) = \frac{\text{activity}_{\text{immo.}}}{\text{protein loading}} \quad (6)$$

$$\text{Activity yield (\%)} = \frac{\text{activity}_{\text{spec.}}\left(\text{U mg}_{\text{immo.}}{}^{-1}\right) \times m_{\text{immo.}}\left(\text{mg}_{\text{enzyme}}\right)}{m_{\text{offered}}\left(\text{mg}_{\text{enzyme}}\right) \times \text{activity}_{\text{spec.}}\left(\text{U mg}_{\text{free}}{}^{-1}\right)} \times 100 \quad (7)$$

Assessment of the thermal stability of free and immobilized enzymes. 1 mL of the free enzyme dilution (1 : 1000) or an appropriate amount of the respective heterogenized enzyme (40 mg) in 1 mL sodium phosphate buffer (100 mM, pH 7.5) was incubated at 30, 40, 50, 60, and 70 °C. Periodically, samples were withdrawn and their residual activities were measured *via* the enzyme activity assay. The initial activity was set to 100% and the deactivation constant was calculated from the obtained slopes. The half-life time ($t_{1/2}$) was calculated with eqn (8).

$$t_{1/2}\ (\text{h}) = \frac{\ln 2}{k_{\text{d}}} \quad (8)$$

Recycling analysis of the immobilized enzymes. For the recycling analysis, the immobilized enzyme on the wetted carrier (10 mg) was placed in a cuvette containing sodium phosphate buffer (100 mM, pH 7.5, 990 μL) and the substrate *p*-nitrophenyl acetate (10 μL, 10 mM in DMSO). Afterwards, the enzyme activity was determined as described in the respective section. Thereafter, the activity assay solution was centrifuged, decanted and washed three times with sodium phosphate buffer. The overall procedure was repeated until no enzyme activity was observed.

Proof-of-concept reaction: kinetic resolution of (*R*,*S*)-1-phenylethanolacetate to (*R*)-1-phenylethanol and (*S*)-1-phenylethanolacetate. The reaction conditions and method were adapted and modified from Meyer *et al.*[36] For reaction time progressive curves: 50 mM *rac*-1-phenylethanolacetate **14** (yielding 25 mM of each enantiomer in solution) and 10 U of *Ca*lB (corresponding to 15.6 μL cell free extract [642 U $\text{mL}_{\text{CFE}}{}^{-1}$] or 173.6 mg heterogenized *Ca*lB on hydrogel particles carrier II [2.7 U $\text{g}_{\text{carrier}}{}^{-1}$]) were added to 10 mL of potassium phosphate buffer (100 mM, pH 7.5) in a glass vial. The reaction mixture was shaken at 30 °C in a thermomixer at 500 rpm for a total reaction time of 24 h. Samples were withdrawn at intervals and analyzed by gas chromatography (GC). For sampling, 500 μL of reaction solution was extracted in 500 μL dichloromethane (DCM) and the organic phase was then analyzed *via* GC.

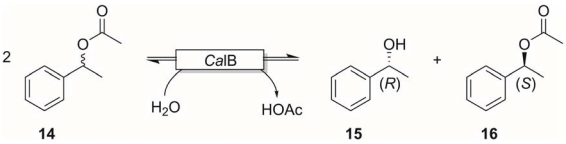

Scheme 8 Kinetic resolution of (*R*,*S*)-1-phenylethanolacetate to (*R*)-1-phenylethanol and (*S*)-1-phenylethanolacetate.

Recycling studies. In individual triplicates, the reaction was performed with 10 U of immobilized *Ca*lB on carrier III with 50 mM *rac*-1-phenylethanolacetate **14** at a 10 mL scale with potassium phosphate buffer (100 mM; pH 7.5) at 30 °C as described above. After 24 h, a 500 μL sample of the heterogeneous reaction mixture was taken, extracted with the same amount of DCM, and subsequently, the remaining reaction mixture was separated by centrifugation. To maintain the ratios of heterogenized carrier to reaction volume, 10 mL minus the total withdrawn sample amount was freshly added, and 50 mM of the substrate **14** was supplemented again to start a new reaction cycle for a further 24 h (Scheme 8).

Gas chromatography (GC) conditions. The conversion of *S*-**14** and enantiomeric excess (ee) values of **15** and **16** in all reactions were measured by GC (Shimadzu GC-2030) with a flame ionization detector (FID). For this method, a cyclodextrin column CP-ChiraSil-Dex CB (25 m × 0.25 mm, 0.25 μm diameter) was used. The measurements were performed at 120 °C for 10 min, followed by a heating rate of 30 °C min^{-1} to 190 °C. The temperature was held for 3 min, and the column flow was held constantly at 1 mL min^{-1}. Conversions and enantiomeric excesses were calculated by integrating and comparing the respective peak areas. Retention times were determined with the authentic reference material.

Results and discussion

Synthesis and characterization of the immobilization matrix

Enzyme immobilization onto polymer carriers typically requires pre-modification or activation of the surface with highly reactive groups to allow the immobilization reaction to occur under mild conditions, thereby protecting the enzyme from severe denaturation. To achieve this activation, different strategies are used in the literature: applying glycidol, thionyl chloride, 4-dimethylaminopyridine, cyanuric chloride, cyanogen bromide, or disuccinimidyl suberate. In this work, we synthesized poly(-aspartic acid) (PASP) hydrogel particles, starting from aspartic acid over polysuccinimide (PSI) through polycondensation. The alkaline ring-opening reaction from PSI to PASP was proven by IR (Fig. 1A; significant changes are highlighted in grey). While comparing these two IR spectra, significant bands of N–H stretching (3267 cm^{-1}) and O–H stretching (3066 cm^{-1}) appear only in the PASP spectrum, whereas the C–H stretching band at 2941 cm^{-1} is visible in both spectra. Additionally, there are only two C=O stretching bands (1797 cm^{-1} and 1705 cm^{-1}) in the

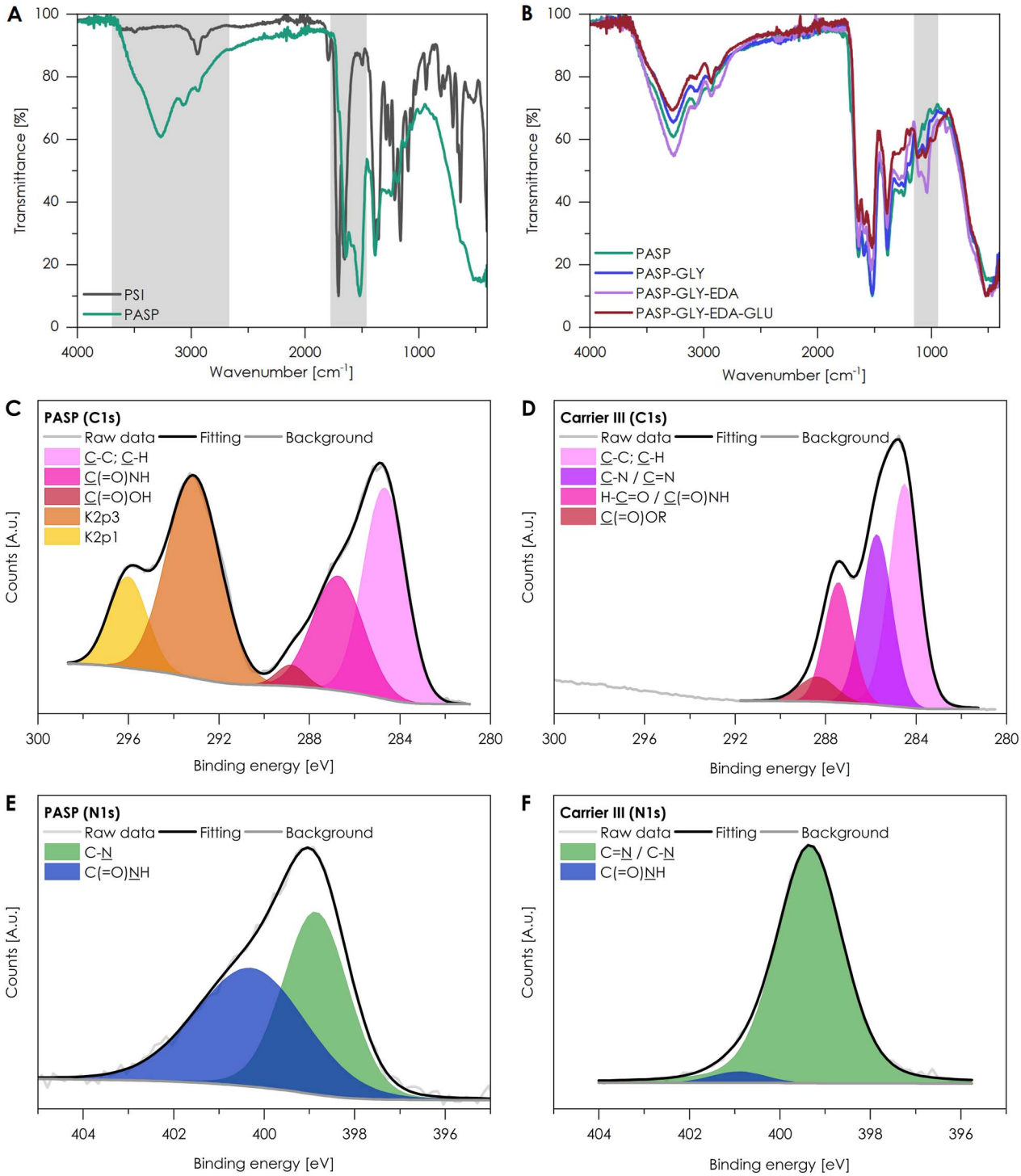

Fig. 1 IR spectra of (A) the PSI crystals and PASP particles, as well as (B) the PASP particles compared to every functionalization step of carrier III. And high-resolution X-ray photoelectron spectroscopy (XPS) measurements of (C) C1s of PASP, (D) C1s of carrier III (PASP-GLY-EDA-GLU), (E) N1s of PASP, and (F) N1s of carrier III.

PSI spectrum, whereas PASP should show six different C=O stretching vibrations. These C=O stretching bands overlap in the PASP spectrum, resulting in a broad C=O band from 1639 cm^{-1} to 1519 cm^{-1}. The spectra of the functionalized PASP particles to carrier III are shown in Fig. 1B. The 1105 to 1037 cm^{-1} range is the C–N stretching vibration of amines. Although the bands in the PASP spectrum are negligible, the bands in the spectra of PASP-GLY-EDA and the carrier III PASP-GLY-EDA-GLU are stronger. These vibrations are primarily due to the introduction of ethylenediamine (EDA) later in the functionalization. The functionalization of the PASP particles was also validated by XPS (Fig. 1C–F). The C1s signal of PASP can be

Table 1 XPS data overview of the C1s and N1s from PASP and carrier III (PASP-GLY-EDA-GLU)

Element	PASP [eV]		Carrier III (PASP-GLY-EDA-GLU) [eV]	
C1s	C–C; C–H	284.68	C–C; C–H	284.52
	C(=O)NH	286.74	C–N/C=N	285.73
	C(=O)OH	288.82	H–C=O/C(=O)NH	287.43
	K2p3	293.12	C(=O)OR	288.37
	K2p1	296.02		
N1s	C–N	398.86	C=N/C–N	399.34
	C(=O)NH	400.29	C(=O)NH	400.91

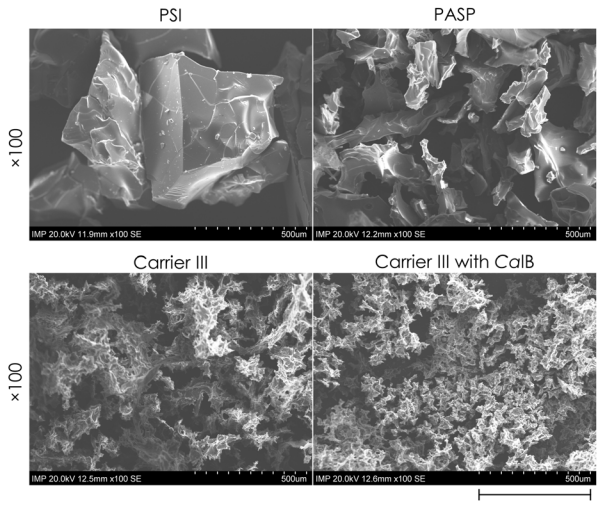

Fig. 2 SEM images of the PSI, PASP, and carrier III with and without immobilized *Cal*B (scale bar 500 μm).

fitted into three peaks at 284.68, 286.74, and 288.82 eV corresponding to C-C, amide (N–C=O), and carboxylic (COOH) groups, respectively (Table 1).[37,38] Two additional peaks appear at higher binding energies of 293.12 and 296.02 eV, corresponding to traces of potassium ions present in the PASP sample, and are not present in the carrier III sample. The C1s signal of carrier III shows an additional peak at 285.73 eV corresponding to C=N and C–N.[39] The peak at 288.37 eV could be attributed to ester group formation in carrier III. The chemical shift towards lower binding energy of around 0.45 eV compared to the carboxylic group of the non-functionalized PASP indicates the functionalization of PASP through esterification of the carboxylic group.[40] The peak at 287.43 eV can be attributed to the presence of the aldehyde group in addition to the amide group from the PASP backbone.[41] The N1s region of the photoelectron spectra was also investigated; the peaks at 398.86 and 400.29 eV of the PASP sample correspond to C–N and O=C–N from the amide functional group of PASP.[42,43] The broad peak at 399.34 eV of the N1s signal of carrier III can be attributed to the presence of C–N and C=N functional groups in the structure.[44] The peak at 400.91 eV could be due to the O=C–N group shifting to higher binding energy after PASP functionalization.[45]

In summary, the opening of the PSI rings was detected by observing the band shift and the broadening of the C=O stretching vibration and the additional O–H stretching vibration. The process of functionalization of PASP could be observed through the analysis of the C–N stretching vibration. These findings were additionally validated by XPS, showing significant signals for C=N and C=N/C–N.

Additionally, the surface morphology of the precursor PSI, the hydrogel PASP, and the carrier III (PASP-GLY-EDA-GLU) was examined by SEM analysis (Fig. 2). After crosslinking and hydrolysis of PSI, the PASP hydrogel cylinders were ground into

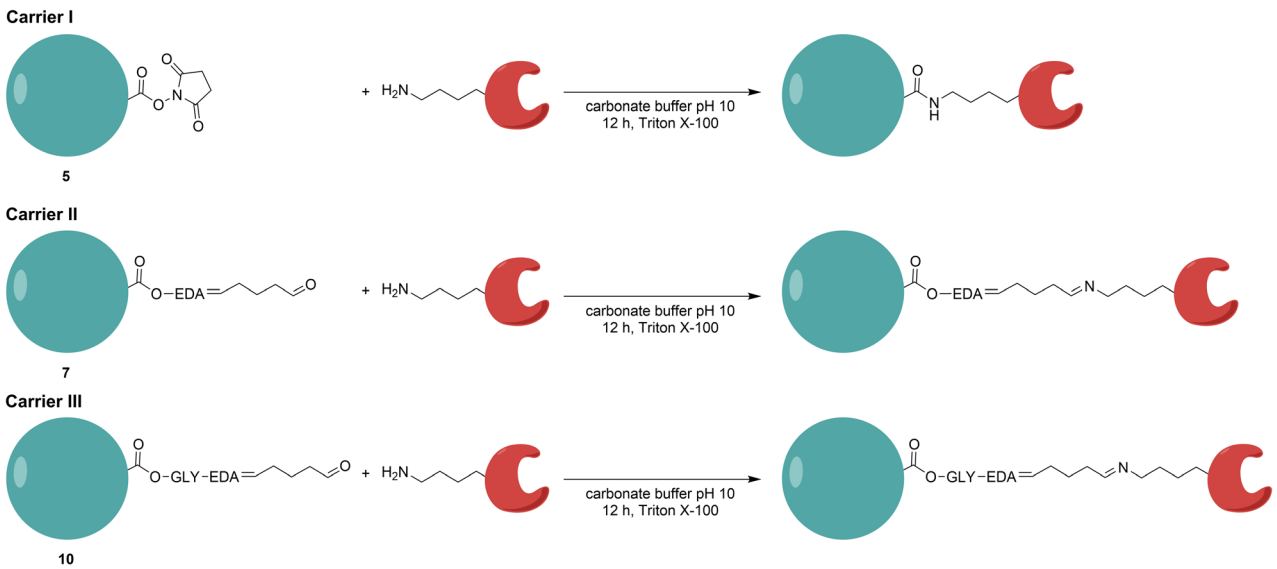

Scheme 9 Schematic illustration of the different functionalized immobilization carriers using the NHS-ester activated PASP (carrier I: PASP-EDC/NHS), the NHS-ester activated and ethylenediamine/glutaraldehyde functionalized PASP (carrier II: PASP-EDA-GLU), as well as the glycidol activated and ethylenediamine/glutaraldehyde functionalized PASP (carrier III: PASP-GLY-EDA-GLU) for the immobilization of *Cal*B.

particles around 250 to 500 μm in the dried state. The particles of the functionalized carrier III (PASP-GLY-EDA-GLU) and carrier III with the immobilized enzyme *Ca*lB exhibit much smaller particle sizes ≤250 μm. This phenomenon can be attributed to the harsh reaction conditions that prevail during the functionalization of the particles. The particles can break apart, especially during the gas development of some reaction steps. However, it is essential to note that the size of the particles in the dried state is not comparable to their actual size in an aqueous environment. Therefore, the degree of swelling in ultrapure water and KPi buffer was determined, which suggests that the particles are approximately ten times larger in the swollen state (Fig. S20†).

Characterization of the immobilized enzyme *Ca*lB on the different carriers and the comparison to the free enzyme

The synthesized and functionalized hydrogel particles were applied for the covalent immobilization of enzymes *via* the amino groups of the lysine residues on the enzyme's surface (Fig. S26†). This is illustrated schematically in Scheme 9. To confirm covalent immobilization and exclude merely adsorbed enzyme, the hydrogel carrier was thoroughly washed. Additionally, ATR-IR spectroscopy was performed on the dried hydrogel carrier with the immobilized enzyme, comparing it to a carrier without enzyme (see Fig. S13†). We observed a decrease in the relative intensity of the C=O vibration around 1590 cm^{-1} after immobilization. This suggests that the glutaraldehyde residues reacted with the lysine groups of the enzyme, indicating successful covalent bonding. During immobilization, it became evident that not all linkers were compatible. For instance, the carrier I, the shortest linker, could not immobilize *Ca*lB (Table 2). The investigation focused on the recyclability and thermal stability of the immobilized enzyme in comparison to its free counterpart (Fig. 3). The stability of *Ca*lB on carrier II was outstanding, exceeding the half-life at 30 °C of free *Ca*lB by a factor of 2.6. *Ca*lB, immobilized on carrier II, was also used in up to eight cycles, with relative activity being observed. A drop-in activity during the recycling experiments due to leaching of the enzyme can be ruled out by the preceding washing steps. A drop can rather be attributed to a loss of carrier particles that are too small. This effect is particularly large here, as the recycling experiments were carried out on a very small scale. Seeing that the protein loading of all carriers was low (0.09 ± 0.01–0.47 ± 0.04 $mg_{protein}\ g_{carrier}^{-1}$), these results are still satisfactory when compared to other immobilization strategies in or on hydrogels. Silva *et al.* achieved the covalent immobilization of *Ca*lB on chitosan-based hydrogels, employing diverse covalent linker methodologies, which resulted in immobilized *Ca*lB activities within the same range as those observed in our studies.[33] However, the strategy of covalent immobilization on hydrogels had a significant positive effect on the immobilized enzymes compared to entrapment in hydrogels. In our previous study, in which we immobilized UPO in hydrogels by entrapment, only a markedly lower activity could be detected in the hydrogel pellets (0.32 U $g_{carrier}^{-1}$).[18]

Table 2 Screening results obtained for the covalent immobilization of *Ca*lB on the novel hydrogel-based carriers (ND = not detectable)

	Carrier	Protein loading ($mg_{protein}\ g_{carrier}^{-1}$)	Immobilisation yield (%)	$Activity_{immob.}$ (U $g_{carrier}^{-1}$)	Activity yield (%)
*Ca*lB	I	ND	ND	ND	ND
	II	0.47 ± 0.04	29.0 ± 2.5	2.7 ± 0.3	1.2 ± 0.1
	III	0.28 ± 0.14	27.3 ± 14.2	1.6 ± 0.1	1.1 ± 0.1

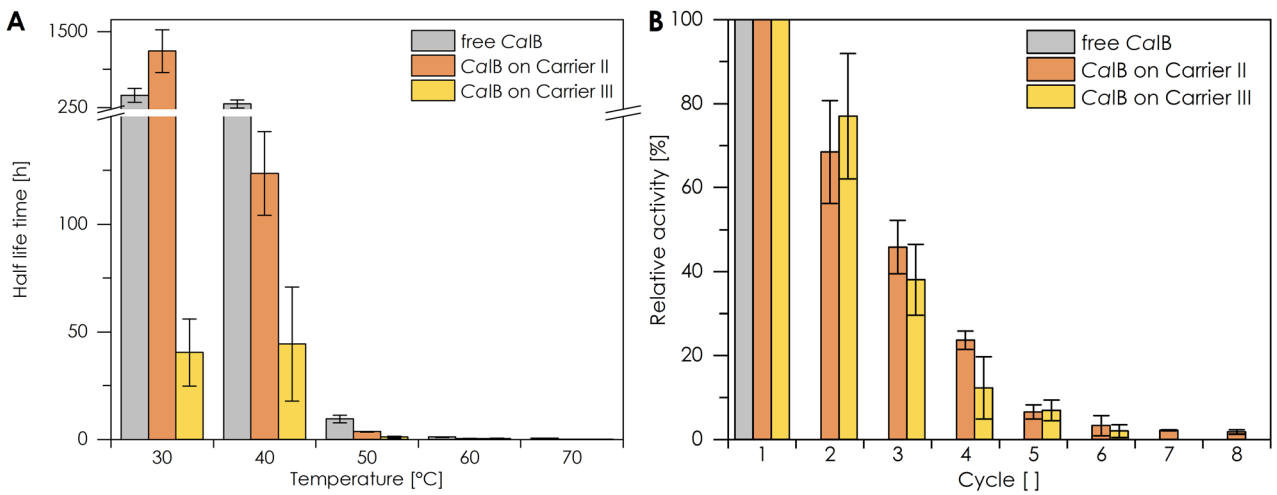

Fig. 3 Overview of (A) the half-life times and (B) the recyclability experiments of *Ca*lB on the previously discussed carriers compared to their corresponding free enzyme. All data plots of the half-life times are shown in the ESI ($n \geq 3$).† The relative activity (%) was determined using *p*-nitrophenyl acetate as the substrate, as described above.

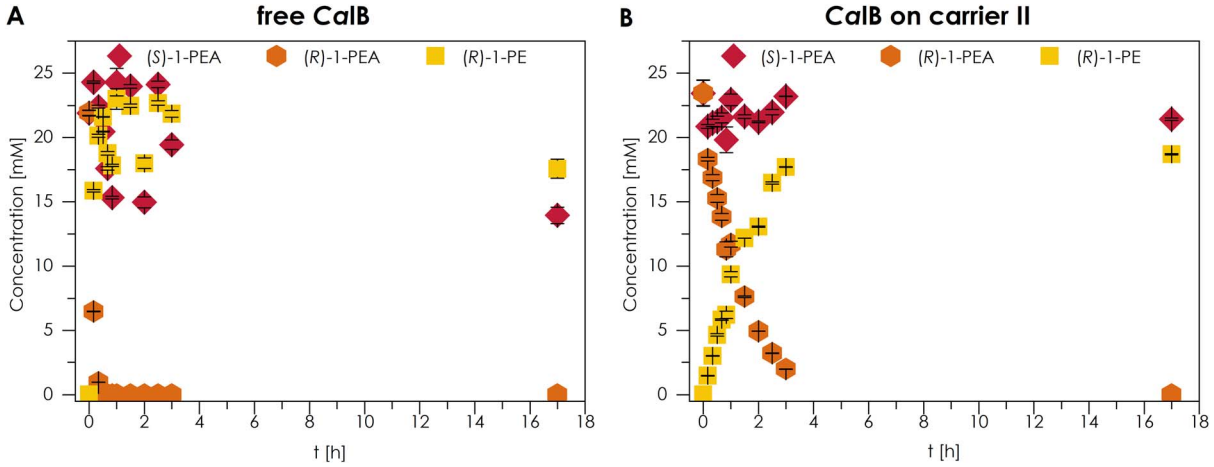

Fig. 4 Comparison of the kinetic resolution of (*R*,*S*)-1-phenylethanolacetate as a proof-of-concept reaction with (A) the free enzyme *Ca*lB, and (B) the immobilized enzyme *Ca*lB on carrier II. Reaction conditions: immobilized *Ca*lB with 10 U in 10 mL reaction buffer (50 mM KPi, pH 7.5) with 50 mM racemic substrate. All experiments were carried out in duplicate at 30 °C.

Proof of concept reaction: kinetic resolution of (*R*,*S*)-1-phenylethanolacetate to (*R*)-1-phenylethanol and (*S*)-1-phenylethanolacetate

In the present study, an immobilization method was subjected to a proof-of-concept reaction. To achieve this aim, the kinetic resolution of (*R*,*S*)-1-phenylethanolacetate (1-PEA) was catalysed by the immobilized *Ca*lB on carrier II and compared to the free enzyme (Fig. 4). The conversion of (*R*)-1-phenylethanol (1-PE) with free *Ca*lB was 72% after a reaction time of 2 h. *Ca*lB immobilized on the hydrogel particles attained a comparatively lower conversion of 52%. This disparity in enzyme activities leading to lower substrate conversions could be attributed to the diffusion limitation of the substrate and product into the polymeric structure of the hydrogel particles.[18] Since the method presented here relies on the covalent immobilization on the surface of the particles and not on the entrapment of the enzyme within the hydrogel, this could only be a minor factor. Another factor, which may be the dominant one, is the reduced molecular flexibility of *Ca*lB, which has multiple covalent attachments (Fig. S26†) to the hydrogel particles. Furthermore, the enantiomeric excess (ee) values of the kinetic resolution with both the free and immobilized enzymes were determined (see Fig. S30†). In the reaction with free CalB, an ee of >99.9% and an *E*-factor of >200 were achieved after a mere 30 min. In contrast, the *E*-factor of immobilized *Ca*lB did not exceed 200 until the measuring point of 27.5 h. Consequently, it can be hypothesized that the enantioselectivity remains unaffected by the immobilization process; however, the rate of the reaction may be influenced by factors such as kinetics, film, and/or pore diffusion limitations. It can therefore be concluded that the reaction is highly enantioselective.

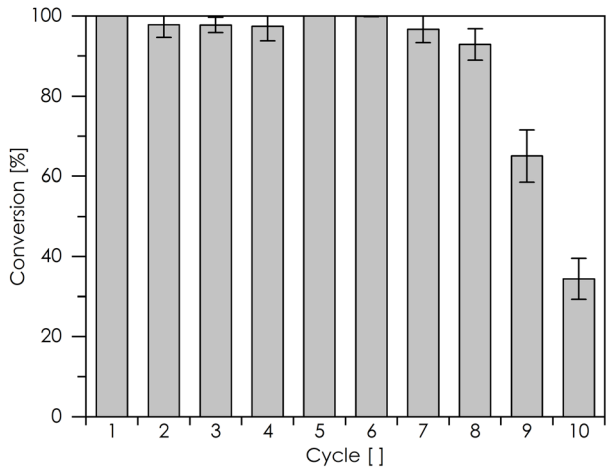

Fig. 5 Conversion of (*R*)-1-phenylethanol during the recycling experiments with the immobilized *Ca*lB on carrier II: recycling immobilized *Ca*lB with 10 U in 10 mL reaction buffer (KPi, pH 7.5, 50 mM) with 50 mM racemic substrate. Each cycle has a reaction time of 24 h. All experiments were carried out in duplicate at 30 °C.

The effects were further intensified in a second run of the kinetic resolution reaction, with a conversion of 15% achieved during recycling after a reaction time of 2 h. Yet again, the complete conversion of the (*R*)-enantiomer within less than 30 h to the (*R*)-ester product is possible (Fig. S27†).

Overall, the immobilized enzyme could be recycled on carrier II and reused for the kinetic resolution (Fig. 5). It was found that the reaction could be catalyzed up to seven times with the immobilized enzyme, achieving full conversion of 1-PE in each of those cycles. A substantial decline in conversion after the seventh cycle was observed; *e.g.*, the 10th cycle gave a conversion of only 34%. The full conversion to the enantiopure (*R*)-ester achieved in seven consecutive reactions shows the promising potential of the here-developed immobilization strategy.

Conclusions

The present study investigated the covalent immobilization of *Ca*lB on hydrogel-based carriers composed of poly(aspartic acid), as a biodegradable, water-soluble condensation polymer. The carriers were synthesized from poly(aspartic acid) hydrogel

particles and functionalized with common strategies in enzyme immobilization. The newly designed carriers were successfully characterized and analyzed *via* ATR, Raman, XPS, and SEM.

The NHS-ester or epoxy-activated hydrogel particles were functionalized with different linkers, resulting in three carriers with varying linker lengths for immobilization targeting the lysine groups of the enzymes. We selected glycidol, EDA, and glutaraldehyde as linkers because of their unique properties, which improve the immobilization and functionality of enzymes. Glycidol's short linker length and reactive epoxide group provide high functionalization of our PASP carrier. EDA offers a short, bifunctional span that fosters strong binding through its reactive amine groups. Glutaraldehyde's longer, flexible structure provides additional spacing to accommodate larger enzymes and facilitate versatile orientations. Its dialdehyde groups react effectively with amino groups on enzymes and their carrier counterparts, ensuring robust cross-linking.

The study revealed major variations in activity among the three linker lengths, as well as the necessity of identifying distinct optimal linkers. While *Ca*lB showed no activity on carrier I, it showed significant activity on carrier II and carrier III (2.7 U $g_{carrier}^{-1}$ and 1.6 U $g_{carrier}^{-1}$, respectively). The stability of *Ca*lB on carrier II was found to be exceptional, with a half-life at 30 °C that was 2.6 times greater than that of free *Ca*lB. Furthermore, *Ca*lB immobilized on carrier II demonstrated a capacity to undergo up to eight cycles, with relative activity observed during this period.

Although this study focused mainly on the thermal stability of enzymes, it has been reported that immobilization in hydrogels can lead to increased tolerance of temperature and pH variations compared to free enzymes.[7,46] Many studies have reported this enhanced process stability, storability, and resistance to pH and temperature, suggesting that the hydrogel beads or capsules generally function as a physical barrier protecting the encapsulated enzyme.[8,47–49]

The proof-of-concept reaction of immobilized *Ca*lB on carrier II for the kinetic resolution of (*R*,*S*)-1-phenylethanol acetate demonstrated the capacity to perform up to seven cycles without a substantial decline in product yield, corresponding to an operational duration exceeding 200 hours, underscoring the promising applicability of these new generation hydrogel-based enzyme carriers. However, it is also important to acknowledge the limitations of this method. Generally, only low protein loading was achievable with the three immobilization methods. In addition to the loss of activity compared to the free enzyme or strong structural rigidity due to multiple covalent bonds, the handling of hydrogel particles is also a concern. Grinding the hydrogel can lead to the production of particles with a wide range of sizes. Particularly small particles (providing high surface area) settle poorly during centrifugation, making them more difficult to recycle. Therefore, future efforts will be focused on achieving a more precise production of hydrogel particles.

The scalability and economic viability of producing PASP-based carriers largely depend on the cost and availability of key starting materials, such as glutaraldehyde, aspartic acid, ethylenediamine, glycidol, EDC, and NHS. Aspartic acid is cost-effective and abundant, while ethylenediamine and glutaraldehyde are also relatively inexpensive, supporting large-scale production. However, EDC and NHS are specialized reagents that may increase production costs. The synthesis of the precursor PSI *via* polycondensation could be further upscaled, and the cost of raw materials is not an issue. However, it is crucial to ensure adequate mixing of the increasingly hardening polymer during the reaction, possibly using a kneader reactor, and to ensure the removal of water with a water separator.

The effective covalent immobilization of lipase *Ca*lB on tailored hydrogel carriers marks a notable advancement, offering promising potential for technical applications. One key application lies in the realm of fine chemical synthesis, where the precise control offered by our immobilized enzyme can ensure the production of high-purity products, which is critical in pharmaceutical manufacturing and specialty chemicals. The robustness and recyclability of the immobilized *Ca*lB can lead to more cost-effective and sustainable processes by enabling repeated use of the biocatalyst, reducing both waste and production costs. This feature is particularly advantageous in large-scale operations where enzyme longevity is crucial. Additionally, the versatility of our hydrogel carrier platform can be extended to other enzymes. By targeting lysine groups of other enzymes or, if not applicable, modifying the functionality on the carrier surface, this system could be adapted to catalyze a broad range of reactions, facilitating innovation across various sectors. Additionally, the interaction between the desired enzyme and the selected linker length could be analyzed in more detail based on the presented results. This analysis could facilitate the selection of a suitable covalent immobilization method for other types of enzymes for future studies.

Data availability

The data supporting this article have been included as part of the ESI.†

Author contributions

Johanna Meyer: conceptualization, investigation, methodology & writing – original draft; Lars-Erik Meyer: investigation, methodology & writing – original draft; Hadir Borg: investigation & writing – original draft; Dirk Dorfs: funding acquisition & writing – review and editing; Selin Kara: funding acquisition & writing – review and editing. All authors approved the final version of the manuscript.

Conflicts of interest

There are no conflicts to declare.

Acknowledgements

SK thanks the Ministry for Science and Culture for Lower Saxony for the Holen & Halten starting grant (grant no. 12.5-76251-17-9/20) and Aarhus Universitets Forskningsfond (AUFF, grant no. AUFF-T-2018-7-11) for the financial support. HB would like to

thank the Cluster of Excellence PhoenixD (EXC 2122, Project ID 390833453) for the funding support from the Deutsche Forschungsgemeinschaft (DFG, German Research Foundation) under Germany's Excellence Strategy and for providing the XPS device. Additionally, we want to thank Martina Weiß, Caroline Müller, Martin Pähler, and Enes Yayci for their support in the daily laboratory routine. Furthermore, we thank Sven Barker for his help with the SEM images, Marek Biermann from Anton Paar OptoTec GmbH (Seelze, Germany) for his help with the Raman spectra, and Jan Biedermann, Nele Peters, Jona Bauer, Katharina Naerger, Marco Matosevic, and Tom Kunde for their assistance in the lab.

References

1 R. A. Sheldon, *Adv. Synth. Catal.*, 2007, **349**, 1289–1307, DOI: 10.1002/adsc.200700082.
2 P. de Santis, N. Petrovai, L. E. Meyer, M. Hobisch and S. Kara, *Front. Chem.*, 2022, **10**, 1–10, DOI: 10.3389/fchem.2022.836597.
3 E. Krisch, D. Balogh-Weiser, J. Klimkó, B. Gyarmati, K. László, L. Poppe and A. Szilágyi, *eXPRESS Polym. Lett.*, 2019, **13**, 512–523, DOI: 10.3144/expresspolymlett.2019.43.
4 A. K. Dwamena, S. H. Woo and C. S. Kim, *Biotechnol. Lett.*, 2020, **42**, 845–852, DOI: 10.1007/s10529-020-02829-w.
5 D. Magnin, S. Dumitriu and E. Chornet, *J. Bioact. Compat. Polym.*, 2003, **18**, 355–373, DOI: 10.1177/0883911503038375.
6 J. Meyer, L.-E. Meyer and S. Kara, *Eng. Life Sci.*, 2022, **22**, 165–177, DOI: 10.1002/elsc.202100087.
7 M. Bilal and H. M. N. Iqbal, *Int. J. Biol. Macromol.*, 2019, **130**, 462–482, DOI: 10.1016/j.ijbiomac.2019.02.152.
8 H. Hang, C. Wang, Y. Cheng, N. Li and L. Song, *Appl. Biochem. Biotechnol.*, 2018, **184**, 453–470, DOI: 10.1007/s12010-017-2558-5.
9 D. I. Torres, M. E. Villanueva, J. M. Lázaro-Martínez, G. J. Copello and V. Campo Dall' Orto, *Cellulose*, 2018, **25**, 1657–1672, DOI: 10.1007/s10570-018-1684-8.
10 S. Sondhi, R. Kaur, S. Kaur and P. S. Kaur, *Int. J. Biol. Macromol.*, 2018, **117**, 1093–1100, DOI: 10.1016/j.ijbiomac.2018.06.007.
11 S. Raghu and G. Pennathur, *Turk. J. Biol.*, 2018, **42**, 307–318, DOI: 10.3906/biy-1805-28.
12 P. Fernandes, M. P. Marques, F. Carvalho and J. M. Cabral, *J. Chem. Technol. Biotechnol.*, 2009, **84**, 561–564, DOI: 10.1002/jctb.2080.
13 E. Pişkin, *Int. J. Artif. Organs*, 1984, **7**, 283–288, DOI: 10.1177/039139888400700511.
14 G. Bayramoğlu, B. Kaya and M. Y. Arıca, *Food Chem.*, 2005, **92**, 261–268, DOI: 10.1016/j.foodchem.2004.07.022.
15 F. Ayhan, H. Ayhan, E. Pişkin and A. Tanyolaç, *Bioresour. Technol.*, 2002, **81**, 131–140, DOI: 10.1016/S0960-8524(01)00114-6.
16 A. Grollmisch, U. Kragl and J. Großeheilmann, *SynOpen*, 2018, **2**, 192–199, DOI: 10.1055/s-0037-1610144.
17 S. Vaupel, R. Mau, S. Kara, H. Seitz, U. Kragl and J. Meyer, *J. Mater. Chem. B*, 2023, **11**, 6547–6559, DOI: 10.1039/D3TB00285C.
18 L.-E. Meyer, D. Horváth, S. Vaupel, J. Meyer, M. Alcalde and S. Kara, *React. Chem. Eng.*, 2023, **8**, 984–988, DOI: 10.1039/D3RE00058C.
19 S. Karboune, A. Archelas, R. Furstoss and J. Baratti, *J. Mol. Catal. B: Enzym.*, 2005, **32**, 175–183, DOI: 10.1016/j.molcatb.2004.11.001.
20 B. L. Krishna, A. N. Singh, S. Patra and V. K. Dubey, *Process Biochem.*, 2011, **46**, 1486–1491, DOI: 10.1016/j.procbio.2011.03.022.
21 A. Erfani, P. Zarrintaj, J. Seaberg, J. D. Ramsey and C. P. Aichele, *J. Appl. Polym. Sci.*, 2021, **138**, 1–11, DOI: 10.1002/app.50545.
22 H. Adelnia, H. D. N. Tran, P. J. Little, I. Blakey and H. T. Ta, *ACS Biomater. Sci. Eng.*, 2021, **7**, 2083–2105, DOI: 10.1021/acsbiomaterials.1c00150.
23 B. Gyarmati, Á. Némethy and A. Szilágyi, *RSC Adv.*, 2014, **4**, 8764–8771, DOI: 10.1039/c3ra47530a.
24 B. Gyarmati, A. Mammadova, G. Stankovits, D. Barczikai and A. Szilágyi, *Period. Polytech., Chem. Eng.*, 2021, **65**, 183–191, DOI: 10.3311/PPch.16869.
25 C. Németh, B. Gyarmati, T. Abdullin, K. László and A. Szilágyi, *Acta Biomater.*, 2017, **49**, 486–494, DOI: 10.1016/j.actbio.2016.11.065.
26 B. Gyarmati, B. Vajna, Á. Némethy, K. László and A. Szilágyi, *Macromol. Biosci.*, 2013, **13**, 633–640, DOI: 10.1002/mabi.201200420.
27 Á. Némethy, K. Solti, L. Kiss, B. Gyarmati, M. A. Deli, E. Csányi and A. Szilágyi, *Eur. Polym. J.*, 2013, **49**, 2392–2403, DOI: 10.1016/j.eurpolymj.2013.02.015.
28 B. Gyarmati, E. Z. Mészár, L. Kiss, M. A. Deli, K. László and A. Szilágyi, *Acta Biomater.*, 2015, **22**, 32–38, DOI: 10.1016/j.actbio.2015.04.033.
29 T. Gyenes, V. Torma, B. Gyarmati and M. Zrínyi, *Acta Biomater.*, 2008, **4**, 733–744, DOI: 10.1016/j.actbio.2007.12.004.
30 B. Á. Szilágyi, Á. Némethy, A. Magyar, I. Szabó, S. Bősze, B. Gyarmati and A. Szilágyi, *React. Funct. Polym.*, 2018, **133**, 21–28, DOI: 10.1016/j.reactfunctpolym.2018.09.015.
31 T. Göckler, S. Haase, X. Kempter, R. Pfister, B. R. Maciel, A. Grimm, T. Molitor, N. Willenbacher and U. Schepers, *Adv. Healthcare Mater.*, 2021, **10**, 2100206, DOI: 10.1002/adhm.202100206.
32 H. L. Bonazza, R. M. Manzo, J. C. S. dos Santos and E. J. Mammarella, *Appl. Biochem. Biotechnol.*, 2018, **184**, 182–196, DOI: 10.1007/s12010-017-2546-9.
33 J. A. Silva, G. P. Macedo, D. S. Rodrigues, R. L. C. Giordano and L. R. B. Gonçalves, *Biochem. Eng. J.*, 2012, **60**, 16–24, DOI: 10.1016/j.bej.2011.09.011.
34 A. A. Mendes, H. F. de Castro, D. de S. Rodrigues, W. S. Adriano, P. W. Tardioli, E. J. Mammarella, R. de C. Giordano and R. de L. C. Giordano, *J. Ind. Microbiol. Biotechnol.*, 2011, **38**, 1055–1066, DOI: 10.1007/s10295-010-0880-9.
35 M. M. Bradford, A Rapid and Sensitive Method for the Quantitation of Microgram Quantities of Protein Utilizing the Principle of Protein-Dye Binding, *Anal. Biochem.*, 1976, **72**(1–2), 248–254.

36 L. E. Meyer, A. Gummesson, U. Kragl and J. von Langermann, *Biotechnol. J.*, 2019, **14**, 1–7, DOI: **10.1002/biot.201900215**.
37 C. Chai, Y. Xu, S. Shi, X. Zhao, Y. Wu, Y. Xu and L. Zhang, *RSC Adv.*, 2018, **8**, 24970–24981, DOI: **10.1039/c8ra03534b**.
38 Y. Yuan, J. Yang, Z. Liu, R. Tan, M. Chuai, J. Sun, Y. Xu, X. Zheng, M. Wang, T. Ahmad, N. Chen, Z. Zhu, K. Li and W. Chen, *Adv. Energy Mater.*, 2022, **12**, 2103705, DOI: **10.1002/aenm.202103705**.
39 X. Yan, T. Xu, G. Chen, S. Yang, H. Liu and Q. Xue, *J. Phys. D Appl. Phys.*, 2004, **37**, 907–913, DOI: **10.1088/0022-3727/37/6/015**.
40 S. R. Leadley, M. C. Davies, M. Vert, C. Braud, A. J. Paul, A. G. Shard and J. F. Watts, *Macromol.*, 1997, **30**, 6920–6928, DOI: **10.1021/ma9702612**.
41 X. Wu, W. Jiang, Y. Luo and J. Li, *J. Appl. Polym. Sci.*, 2019, **136**, 47441, DOI: **10.1002/app.47441**.
42 H. He, Y. Hu, S. Chen, L. Zhuang, B. Ma and Q. Wu, *Sci. Rep.*, 2017, **7**, 3913, DOI: **10.1038/s41598-017-04329-w**.
43 J. S. Stevens, A. C. de Luca, M. Pelendritis, G. Terenghi, S. Downes and S. L. M. Schroeder, *Surf. Interface Anal.*, 2013, **45**, 1238–1246, DOI: **10.1002/sia.5261**.
44 A. Artemenko, A. Shchukarev, P. Štenclová, T. Wagberg, J. Segervald, X. Jia and A. Kromka, *IOP Conf. Ser. Mater. Sci. Eng.*, 2021, vol. 1050, p. 1050, DOI: **10.1088/1757-899X/1050/1/012001**.
45 M. Kehrer, J. Duchoslav, A. Hinterreiter, M. Cobet, A. Mehic, T. Stehrer and D. Stifter, *Plasma Processes Polym.*, 2019, **16**, 1800160, DOI: **10.1002/ppap.201800160**.
46 K. H. Kucharzyk, M. Benotti, R. Darlington and R. Lalgudi, *J. Hazard. Mater.*, 2018, **357**, 498–505, DOI: **10.1016/j.jhazmat.2018.06.036**.
47 J. S. de Lima, M. P. Cabrera, A. A. Casazza and M. F. Da Silva, *Int. J. Biol. Macromol.*, 2018, **118**, 1989–1994, DOI: **10.1016/j.ijbiomac.2018.07.084**.
48 M. Kampmann, A. C. Hoffrichter, D. Stalinski and R. Wichmann, *J. Mol. Catal. B: Enzym.*, 2015, **116**, 124–133, DOI: **10.1016/j.molcatb.2015.03.013**.
49 S. D. Gür, N. Idil and N. Aksöz, *Appl. Biochem. Biotechnol.*, 2018, **184**, 538–552, DOI: **10.1007/s12010-017-2566-5**.